Steel and Composite Structures, Vol. 8, No. 3 (2008) 179-200
DOI: http://dx.doi.org/10.12989/scs.2008.8.3.179

Experimental studies and numerical analysis of the shear behavior of fin plates to tubular columns at ambient and elevated temperatures

M.H. Jones and Y.C. Wang†

University of Manchester, Manchester, UK

(Received December 1, 2007, Accepted April 1, 2008)

Abstract. This paper reports the results of a recent experimental study into the behavior of welded fin-plate connections to both hollow and concrete filled tubular (CFT) columns under shear. Experiments have been performed at both ambient and elevated temperatures with the aid of an electric kiln. The observed failure modes include fracture of the fin plate and tearing out of the tube around the welds. By considering the results of previously published research, the current design method for similar connections under purely tensile load, in CIDECT Guide 9, based on a deformation limit of 3% of the tube width is shown to be inadequate when evaluating the ultimate strength of such connections. By comparing the results from the current test program which failed in the fin-plate with Eurocode guidance for failure of a fin-plate alone under shear and bending load it is shown that the column face influences the overall connection strength regardless of failure mode. Concrete in-fill is observed to significantly increase the strength of connections over empty specimens, and circular column specimens were observed to exhibit greater strength than similarly proportioned square columns. A finite element (F.E.) model, developed using ABAQUS, is presented and validated against the experimental results in order that extensive parametric tests may be subsequently performed. When validating the model against elevated temperature tests it was found that using reduction factors suggested in published research for the specific steel grades improved results over applying the generic Eurocode elevated temperature steel strength reduction factors.

Keywords : concrete filled tubes; fire resistance; joints; elevated temperature; fin plate; experiments; finite element modelling;

1. Introduction

Following recent events such as the World Trade Center building collapse (FEMA 2002) and the Cardington large scale structural fire research program (Wang 2002), the fire behavior of connections has become a prominent research subject. Particularly, the effect of joints on robustness (prevention of progressive collapse) of structures is receiving intensive attention from researchers. The European standard, Eurocode 3 for steel structures (CEN 2003), incorporates some of these computation methods for a variety of welded and bolted connections between steel I-beam and H-columns. There is, however, a comparative lack of research into the behavior of simple welded connections to hollow or concrete-filled tubular (CFT) columns either at ambient or elevated temperatures. CFTs are increasingly used in

†Lecturer, Corresponding author, E-mail : yong.wang@manchester.ac.kr

tall, multi-storey buildings and, as well as pleasing aesthetic properties, they possess structural advantages such as allowing for a comparatively reduced column cross-sectional area and inherent fire-resistance properties due to the insulative properties of the concrete in-fill.

There have been several experimental investigations concerning the interaction between fin-plate and steel hollow section (SHS) under shear load at ambient temperatures. White and Fang (1966) conducted research into the behavior, including shear performance, of five types of welded connections to SHS columns. The closed nature of the column cross-section led White and Fang to conclude that welding was the only practical method for fastening the connection to the tube. The research highlighted the significance of the ratio of width of tube wall to tube thickness. It was noted that as this ratio increases, connections fastened directly to the tube wall tended to become more flexible. Simple plate connections, fillet welded to the tube wall, were observed to produce distortion of the tube wall as the plate rotated under load. When such connections were loaded directly in shear, White and Fang encountered several failure modes in different specimens including local buckling of the tube, weld tearing and web crippling of the connected beam. Sherman (1995) conducted a large series of tests upon realistically loaded framing connections between SHS columns and wide flange beams under predominant shear load. These tests expanded upon those conducted by White & Fang. One limit state was identified for the column face under such load. This limit state was punching shear failure due to the attached beam end rotation when the shear tab connection was thick relative to the SHS wall. The criterion to avoid this failure mode, as described by Packer & Henderson (1997), is to ensure that the tension resistance of the shear tab under axial load (per unit length) is less than the shear resistance of the SHS wall along two planes (per unit length). Thus the thickness of the plate, t_p, is limited with respect to the tube wall thickness, t_0, by the following relationship:

$$t_p < \left(\frac{F_{uO}}{F_{yp}}\right) t_O \tag{1}$$

where F_{u0} is the ultimate stress of the column face and F_{yp} is the yield stress of the connecting plate.

To move from this prescriptive approach and gain a deeper understanding of the behavior of welded fin-plate to tubular column connections, an analytical performance-based approach is required in addition to an experimental results base. More recently, relevant analytical research has been undertaken into tensile behavior of similar connections using the yield-line method to develop design equations. In particular, Yamamoto *et al*. (1994) performed a series of experimental tests and developed a yield line mechanism for transverse branch plate under axial load connected to circular CFTs. It was noted that concrete in-fill significantly increased the strength of such connections. It was also noted that strain distribution for filled tubes was much more localized around the connection than for empty tubes and this was presented as evidence that the resisting mechanism against external forces is different between filled and empty tubes. Thus in developing the mechanism for filled tubes the yield lines were localized in the area of the column face around the connection including the weld. This mechanism was compared with test results and showed fairly good agreement. However, the failure in the experiments was not taken as the ultimate failure load but as a load defined by the General Yield Point Method, shown in Fig. 1 as the load P_p at point B, in which line C is the initial stiffness, line D is half the stiffness and line E is the tangent of the P-δ curve at position A. Therefore, the yield line mechanism of Yamamoto *et al.* does not predict the true strength of such connections which, in their experiments, was

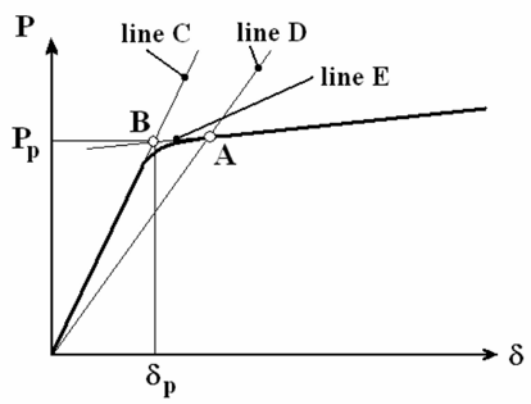

Fig. 1 General Yield Point method (Yamamoto et al. 1994).

observed to be significantly greater than that obtained from the General Yield Point Method. A yield line analysis of such connections to rectangular hollow section (RHS) columns has also been developed by Cao *et al.* (1998) and this work, together with further observations by Kostecki & Packer (2003) appears in the current CIDECT design guide 9 for structural hollow section column connections (Kurobane, Packer, Wardenier & Yeomans 2004). Lu (1997) developed yield line mechanisms for several types of connection including I-beam to RHS columns under in-plane bending moments. The findings of this research are also in the CIDECT guide. The analyses developed by Kostecki & Packer and Lu define the connection strength in terms of a serviceability deformation limit of 1% of the column breadth, b_0, and an ultimate deformation of 3% of b_0. The actual ultimate failure load is not calculated by their analyses.

Furthermore, Lu curve-fitted the initial yield line equations with numerical finite element results. Whilst this approach gives good agreement up to the 3% b_0 deformation limit, it is unclear whether the proposed yield line mechanism is actually developed before failure of the column face is reached. Lu defines the ratio b_0 / t_0 between the column width and thickness as 2γ. For uniplanar welded connections between fin-plates and SHS columns under tensile load it may be observed from the results presented by Lu that relatively thin columns ($2\delta \geq 25$) have an ultimate failure load significantly greater than that at the 3% b_0 limit. However, for thicker columns ($2\gamma = 15.8$ in Lu's tests), the ultimate failure load does not significantly exceed the 3% b_0 load. This suggests that the yield mechanism is under-developed in relatively thick columns. By contrast, the high ultimate loads in the relatively thin tubes suggest a possible membrane action well beyond the 3% b_0 limit. Yield line analysis may not, therefore, be suitable when considering the ultimate deformation of such connections and possible membrane action. Whilst the current CIDECT design guide may give safe answers, it is important to be able to predict the true failure load of joints so that assessment of the potential of progress collapse of structure can be carried out with confidence.

There is also currently a gap in the research regarding the column behavior of such connections. A shear and bending force applied to such a connection implies a tensile force component acting on the column face and this behavior must also be accounted for. The aim of this research program is to contribute to the understanding of the shear behavior of simple connections to CFTs by developing a mathematical method based upon extensive parametric studies. These parametric studies are based on models created using finite element modeling software with the models validated against test results.

This paper presents the results of such a validation. The influence of various parameters such as concrete in-fill and fin-plate geometry upon failure load and failure mode observed in the test program is also discussed.

2. Test program

A series of tests has been performed in order to investigate the interaction between welded T-stubs and both hollow and CFT columns when a shear force is present in the T-stub. The purpose of these tests is also to provide data from which a finite element model for use in extensive parametric studies may be developed and validated against.

2.1 Test set-up

The configuration of the test rig, specimens and instrumentation is described below.

2.1.1 Test rig

The test specimens consisted of T-stubs machined from UB or UC sections fillet welded at the web to the steel tubes, with the T-stub web simulating a fin plate but the T-stub being used for convenience of applying the load. For the specimens with fin plate (T-stub web) thickness, t_f, of 6 mm and 10 mm, a UB section of 203 × 102 × 23 and a UC section of 203 × 203 × 71 respectively were used to manufacture the connections. All column lengths were 450 mm and each connection was welded halfway along the column length and, in the case of SHS sections, breadth. The column lengths were machined from cold-formed tubes of steel grade S355J2H. The machined web of the T-stub section thus simulates a fin-plate and these connections are referred to as such subsequently in this paper. A typical specimen cross-section is depicted in Fig. 2.

The test rig, pictured in Figure 3, consisted of a frame housing a reaction beam. This beam is pinned at one end with the load being applied via a hydraulic jack at the opposite end. The top of the test

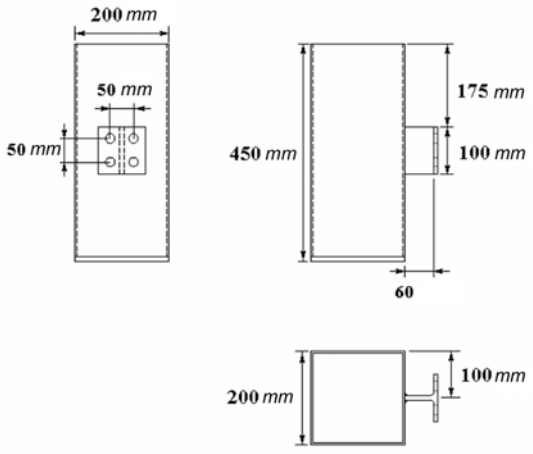

Fig. 2 3-view diagram of typical test specimen

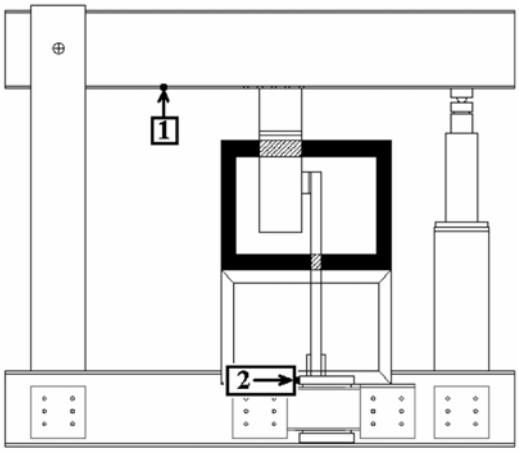

Fig. 3 Test rig with specimen mounted inside kiln

specimen column is anchored to the reaction beam and the T-stub flange of the connection is bolted to a 50 *mm* thick steel hinged strap. This strap is in turn bolted to an assembly forming part of the base of the test rig which is housed on rollers. The roller base and the hinged strap allow rotation of the connection, thereby allowing shear and bending force to be applied to the connection. For the elevated temperature tests an electric kiln was installed with holes cut into the lid and base to allow the specimen to be lowered into the kiln and enclosed. The kiln position is shown as the shaded area in Fig. 3.

2.1.2 Specimen details

The dimensions of the test specimens are detailed in Table 1 in which ambient and elevated temperature tests are prefixed with A and T respectively. The column type has been categorized by the four fundamental variants of the columns tested. These variants are denoted as square hollow section (SHS), square filled section (SFS), circular hollow section (CHS) and circular filled section (CFS). Each circular column section tested has an external diameter of 193.7 mm. Each square section has an external cross-section

Table 1 Test specimen dimensions

Test No.	Column Type	Column Thickness, t_c (mm)	Fin-plate thickness, t_f (mm)	Lever arm (mm)
A1	SFS	5	6	60
A2	CFS	5	10	60
A3	CHS	5	6	60
A4	CHS	5	10	60
A5	SHS	5	6	60
T1	CFS	5	6	30
T2	CFS	12.5	6	30
T3	CFS	5	6	30
T4	CFS	12.5	6	30
T5	SFS	5	6	30
T6	SFS	5	6	30
T7	CFS	5	10	60
T8	CFS	5	10	60

of 200 × 200 mm.

2.1.3 Instrumentation

A number of strain gauges were attached to each ambient test specimen in order to provide data against which to calibrate the F.E. model. Each specimen had five bi-directional and one longitudinal gauge attached to the column face around the connection and two uni-directional gauges attached to the fin-plate perpendicular to the column face. A total of thirteen gauges were attached to Tests A1 through A5 as shown in Fig. 4. External thermocouples were attached to each elevated temperature test specimen at central positions on the rear column face opposite the connection, on one side face of the column and on the fin-plate itself as shown in Fig. 5. Additional internal thermocouples at positions of 25%, 50% and 75% of the column breadth or radius from the connection were placed within specimen T3 as also shown in Fig. 5. The external thermocouples were used as a guide in order that the test load could be applied at the desired specimen temperature. Displacement gauges, with positions and direction 1 and 2 as shown in Fig. 3, were also placed both at a fixed point along the reaction beam and against the roller base in order to give reference points by which to calculate the vertical displacement with load at the

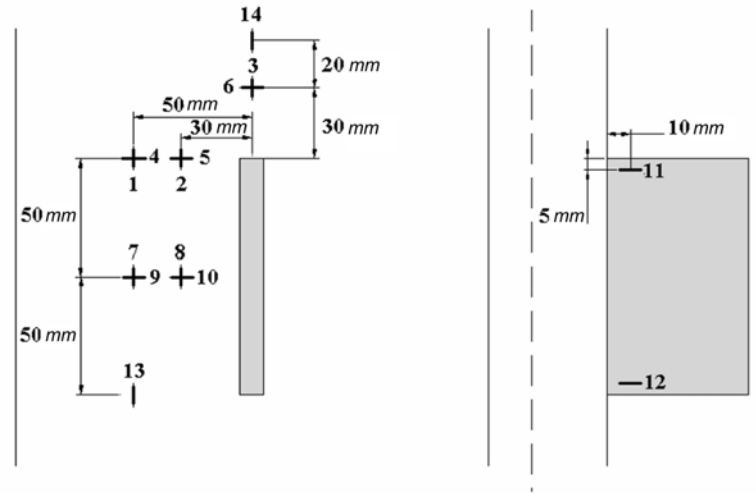

Fig. 4 Strain gauge positions on column face and fin-plate

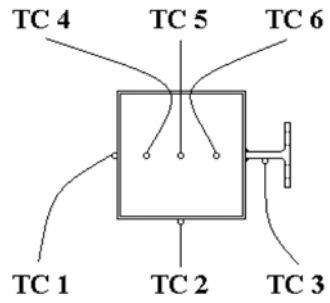

Fig. 5 Thermocouple positions on specimen.

connection using trigonometry. Gauge position 1 varied slightly between tests and these variations were recorded and taken into account when calculating displacement at the connection for each test.

3. Test results observations

The main results of the test program are summarized in Table 2. Two principle failure modes were identified;

(a) Failure of the fin-plate due to bending and shear force (Fig. 6a)

(b) Tear-out failure of the column face around the connection weld (Fig. 6b)

Figure 7 depicts the temperature uniformity throughout loading of Test T3, clearly showing that the desired external test temperature of 600°C was constant throughout. The internal thermocouples within the concrete core reported lower temperatures with the temperature at the core centre about 400°C. Results for thermocouple no. 2 are not included as it malfunctioned during the test. All tests showed

Table 2 Test program results summary

Test No.	Column Type	Test Temperature (°C)	Failure Load (kN)	Failure Mode
A1	SFS	ambient	94.6	(a)
A2	CFS	ambient	163.7	(b)
A3	CHS	ambient	92.5	(a)
A4	CHS	ambient	127.4	(b)
A5	SHS	ambient	69.7	(b)
T1	CFS	400	130.7	(a)
T2	CFS	600	51.1	(a)
T3	CFS	600	49.6	(a)
T4	CFS	500	85.5	(a)
T5	SFS	400	133.8	(a)
T6	SFS	600	53.3	(a)
T7	CFS	600	67.4	(b)
T8	CFS	400	133.4	(b)

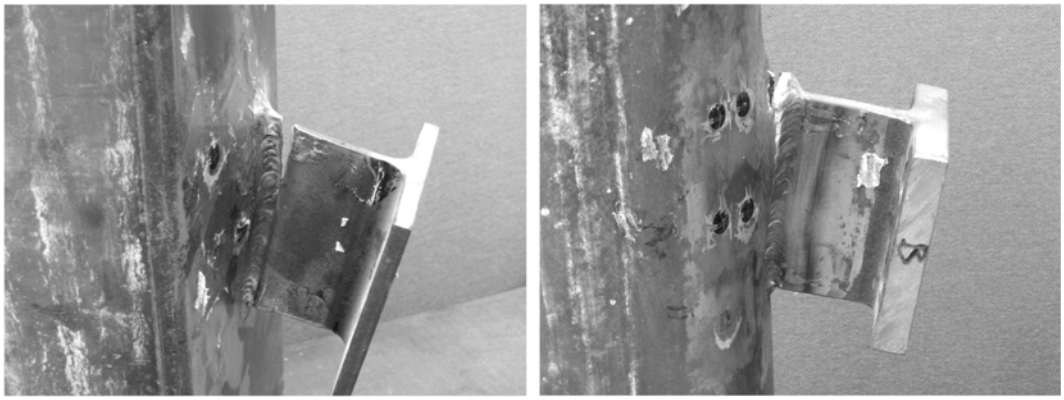

Fig. 6 (a) Failure of the fin-plate by shear & bending (A1) (b) Tear-out of the column face around the weld (A2)

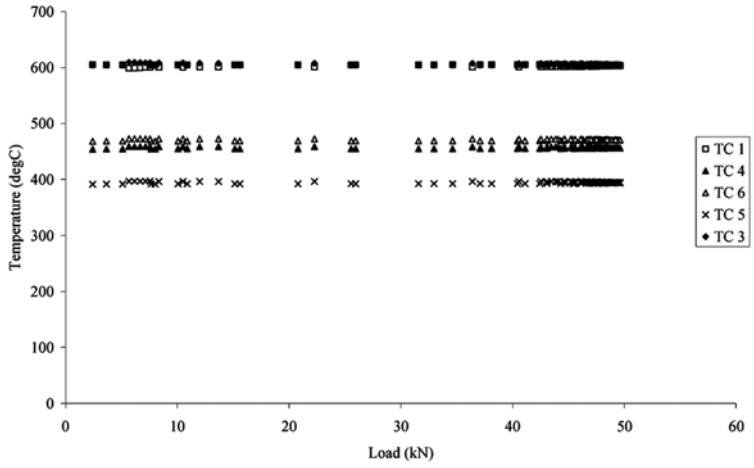

Fig. 7 Temperature distribution throughout test T3

similar uniformity of temperature.

The experimental tests conducted have encompassed several different parameters such as the presence of concrete in-fill, connection lever arm length, temperature, column cross-section and fin-plate to column thickness ratio, t_f / t_c. A discussion of the effects of these parameters and a comparison between similar tests is made below.

3.1 Effect of lever arm and ratio t_f / t_c

As the lever arm of the connection is increased so the applied moment to the column face increases. However, the resistance of the fin-plate to shear and bending force will decrease with increased lever arm. The failure mode is therefore dependant on the relative strengths of the column face and fin-plate. Two lever arm lengths were used in the experiments, 30 and 60 mm. As an example of the effect of varying the lever arm tests A1 and T5 may be compared. Although test T5 was conducted at 400°C, and therefore was weakened in accordance with reduction factors such as those presented in Table 6, the failure load was 41% higher than for the ambient test A1.

The effect of the longer lever arm in test A1 is to significantly weaken the connection relative to the shorter lever arm case even if the latter case is subject to elevated temperatures. In both tests the column strength appears to have been much greater than that of the fin-plate as failure occurred in the fin-plates.

However, when the strength of the fin-plate relative to the column face is increased by, for example, increasing its thickness as in tests A2, A4, T7 and T8, the interaction between the two shifts the failure mode to the column face. Hence the lever arm is important in influencing the relative strength of the fin-plate and column face. As an example illustrating the above observations, the results from similar pairs of tests are compared below.

3.2 Increase in failure load due to concrete in-fill

Test specimens A1 and A5 are both SHS sections with the same fin-plate lever arm of 60 mm. However, it will be observed from Table 2 that the filled specimen, A1, fails at a load 36% higher than that of the empty specimen. Similarly, specimens A2 and A4 are identical in all respects except that of

concrete in-fill. In this case the filled specimen, A2, fails at a load 28% greater than the empty specimen. Hence it may be deduced that the concrete in-fill is influential in determining the failure load of such connections.

The concrete in-fill affects the tension force to the column face by restricting the movement of the column at the base of the connection. The lever arm along the column height may be determined from the strain profile along this length. Since the concrete infill prevents movement of the fin plate at the bottom, for a given shear and bending load, the tension force to the concrete filled tube face must be less than that for the empty tube case. Fig. 8 illustrates this concept with an idealized strain profile along the connection lengths of, (a) an empty column and (b) a filled column. It will be seen that for a given applied shear (F) and bending moment (represented by the lever arm L), the corresponding force, T, acting on the column face will be greater in the empty tube case leading it to fail at a lower value of F than the filled column case since $x_e < x_f$.

In addition to the increased load due to concrete in-fill, the failure mode observed for A1 is different to that of A5 indicating that the concrete in-fill can be influential in determining the failure mode. One way of illustrating the influence of the interaction between column and fin-plate strength upon the failure mode is to compare the theoretical failure of a fin-plate alone under shear and bending force with those test results which failed in the fin-plate. This will first be done for ambient test results as the formula depends upon ultimate steel strength which is reduced with elevated temperature. This reduction is discussed in Section 5.5 of this paper.

Fin-plate failure may be evaluated according to Eurocode 3 (CEN 2001), but is repeated here for clarity. The design plastic shear resistance, $V_{pl,Rd}$, of a plate of cross-section, A, is defined by Eq. 2.

$$V_{pl,\,Rd} = A(f_y/\sqrt{3}) \tag{2}$$

where f_y is the yield stress of the steel.

Eurocode 3 also allows for the influence of combined bending and shear force by noting the reduction in plastic moment capacity due to the presence of shear. This is encapsulated in Eqs. 3 and 4.

$$M_{V,\,Rd} = M_{pl.Rd}\left(1 - \left[\frac{2V_{Sd,fin}}{V_{pl,\,Rd}} - 1\right]^2\right) \tag{3}$$

$$M_{V.Rd} = V_{Sd,fin}.l \tag{4}$$

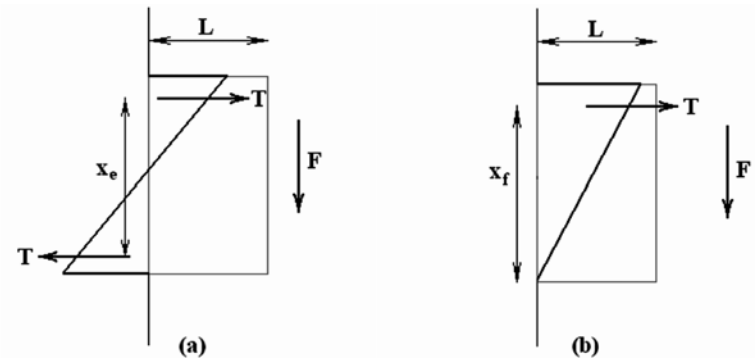

Fig. 8 Idealized strain profile along connection length

where $V_{Sd,fin}$ = resistance in fin plate due to bending and shear; l = lever arm length; $M_{V,Rd}$ = reduced design plastic resistance moment allowing for shear force; and $M_{pl,Rd}$ = design plastic moment resistance.

Table 3 compares the theoretical fin-plate failure and experimental failure load for tests A1 and A3. As the poor correlation from Table 3 shows, it is erroneous to assume that since the failure mode is in the fin-plate, the method for failure of a fin-plate under shear and bending is appropriate. It is apparent that even if the failure mode is in the fin-plate, column deformation prior to failure will exert an influence upon the overall failure load. Fig. 6(a) shows that in test A1 the column face deformed a significant amount before the fin-plate failed.

3.3 Influence of column cross-section

The column cross-section is influential in determining the strength of the column side of the connection and thus the failure mode. Test specimens A3 and A5 are similar in all respects except the column cross-section of A3 is circular with external diameter of 193.7 mm and the square column cross-section of A5 is a similarly sized 200 × 200 mm. However, Test A3 fails at a load 33% greater than Test A5. The failure mode is also different being located in the fin-plate in Test A3 and the column face in Test A5. It may be inferred from these two observations that a circular column face is more resistant to shear and bending loading than the face of a similarly sized square column.

3.4 Results at elevated temperatures

This part of the test program was designed primarily to investigate the effect of temperature upon failure load. The elevated temperature tests were all performed on concrete-filled specimens and the failure load is observed to fall with increased temperature for similar specimen configurations. The test temperatures were all in the range 400°C to 600°C. A guide to this reduction in strength with increased temperature is provided in standards such as Eurocode (CEN 2001). Discussion of these reduction factors in relation to the tests is presented more comprehensively in Section 5.5 of this paper.

Apart from the difference in temperature the same observations can be made for the elevated temperature tests as for the ambient tests. For tests T7 and T8 with the longer lever arm length of 60 mm the failure mode was that of tear-out of the column face around the weld. In these two cases the fin-plate thickness was twice that of the column. For all other specimens, for which the lever arm was 30 mm and the fin-plate thickness smaller relative to the column, the failure mode was shear and bending failure of the fin-plate. The concrete-filled column component of the connection was clearly stronger than the fin-plate, even with the reduced lever arm length.

4. Finite element model

ABAQUS (2004) was used to create the F.E. model. Four basic models with slight variations were created in order to take account of the test specimen column variations, these being circular tube, filled and

Table 3 Comparison of experimental and numerical failure loads for ambient tests

Test no.	Test failure load, T_L (kN)	Theoretical failure load, F_L (kN)	T_L / F_L
A1	94.6	125.3	0.755
A3	92.5	125.3	0.738

unfilled, and square tube, filled and unfilled. In addition, the fin-plate was modified to take account of the different specimen lever arm lengths. In each model the T-stub flange is included to provide a region to which the load, as a body force, may be applied.

4.1.1 Element type

The steel components of each model were constructed using linear shell elements. Shell elements were used because the shell thickness may be easily modified at the input file level, a characteristic which is useful in large-scale parametric studies. They are also less costly in terms of computational resources than solid elements. Modified second order linear elements, with four nodes per side, were also be used for contact analyses as there were convergence problems concerning mid-face nodes in contact arise with the higher order eight-noded quadratic elements. The Riks method, an iterative procedure, was used to obtain the solution.

4.1.2 Circular column model characteristics

The geometry of the model developed for the circular column was dictated by the complexities of solving the 'contact' equations between two surfaces which come together during an analysis. In the particular case of a CFS column, the shell elements modeling the steel column will come into contact with the solid elements representing the concrete core. During analyses conducted in which the nodes of the steel column inner surface and the core outer surface were co-incident in the model space it was noted that 'chattering', where nodes continually open and close in contact without convergence, occurred frequently, often preventing a solution from being reached.

To solve this problem only half of the column cross-section was modeled with the cutting plane restrained by boundary conditions. The column ends (lightly shaded in Fig. 9) were restrained with the Encastre boundary condition and the column edges, AA' and BB', and rear core face along the cutting plane (darkly shaded in Fig. 9) were restrained symmetrically to the y-axis as would be the case if the entire cross-section was modeled. The half-model was compared with full models for several CHS cases and it was found that this did not affect the results. The half-model core for the CFS case was then offset from the shell elements (representing the tube) by a distance of 0.0001 mm in order that the nodes

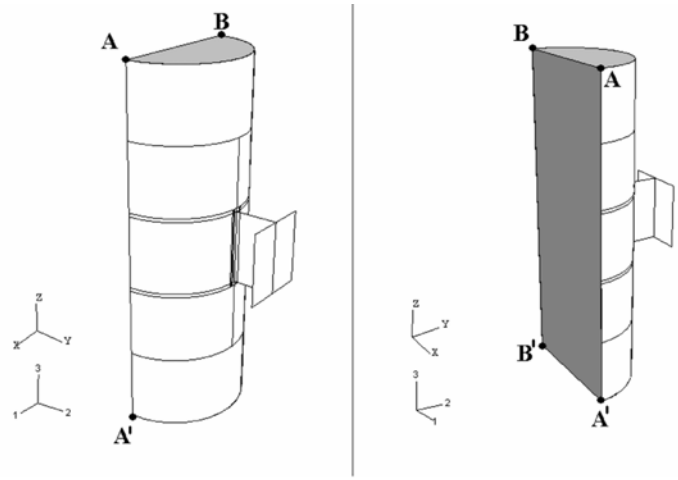

Fig. 9 Boundary conditions for CFS model case

did not share co-incident space at the beginning of the analysis step, thus preventing chattering. The boundary conditions for the CHS model were identical to those of the CFS but with the core section removed.

4.1.3 Square column model characteristics

The square column models were constructed in the same way as the circular sections with the exception that one column face only, that with the connection, was modeled for the SFS case. This was to prevent chattering of the other surfaces of the column with the core. A pinned boundary condition was applied to the column face around the edges AA', A'B', B'B and BA as shown in Fig. 10. The core was modeled in full and restrained at the ends by Encastre boundary conditions. The SHS case was, as with the CHS case, modeled with half the column cross-section restrained by boundary conditions along the cutting plane symmetrical about the y-axis. This cutting plane is shown as edges AA' and DD' in Fig. 11. The SHS ends were modeled with Encastre condition.

Adopting a similar method to Yamamoto *et al.* (1994) and Lu (1997) all models were partitioned around the connection, both in the fin-plate and the column face, in order to simulate the weld footprint. Figure 12 depicts this configuration for the SHS case in which the dark shaded area represents the weld footprint of the column face and the light shaded area that of the fin-plate. This footprint was assigned a slightly thicker thickness than the surrounding material to simulate the physical presence of the weld.

4.2 Material properties

Tensile tests were performed on three coupons from each UB or UC section web and three coupons from each of the column types. The engineering stress-strain data, σ_e-ε_e, obtained was converted to true stress-strain, $\sigma_t - \varepsilon_t$, by the following relationships,

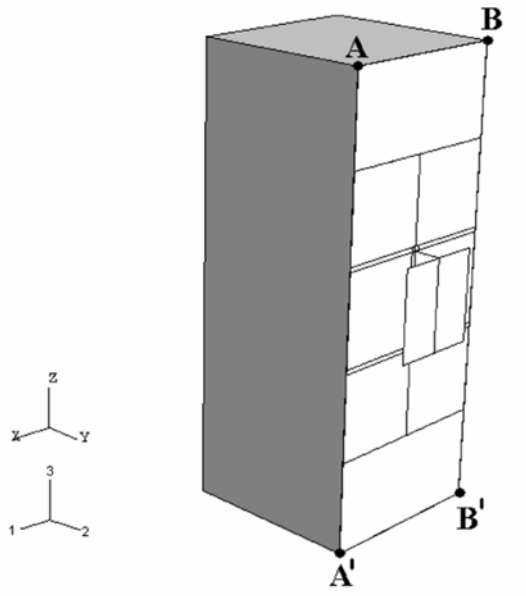

Fig. 10 Boundary conditions for SFS model case

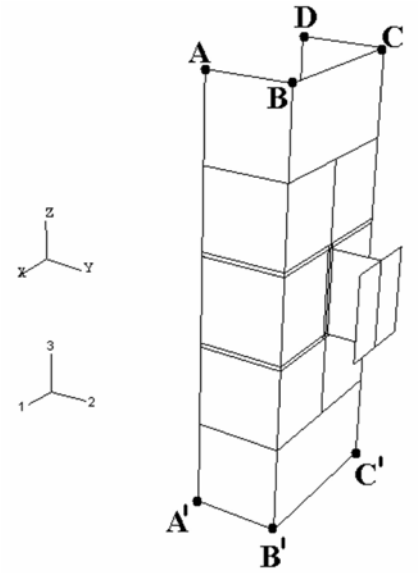

Fig. 11 Boundary conditions for SHS case

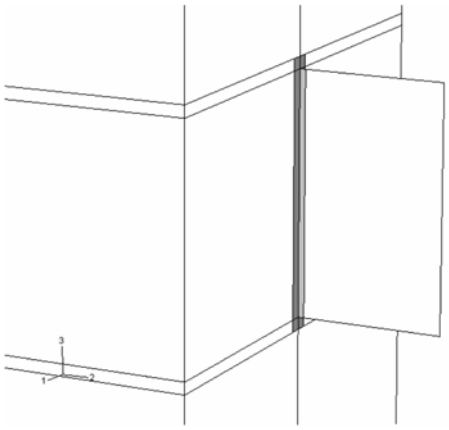

Fig. 12 Area of weld footprint in numerical model

$$\sigma_t = \sigma_e(\sigma_e + 1) \tag{5}$$

$$\varepsilon_t = \ln(\varepsilon_e + 1) \tag{6}$$

For each CFT model the solid core elements were assigned elastic properties equivalent to those of normal strength concrete and fracture of the encased concrete core was not considered at this stage. These simplifications were also practiced by Lu (1997). This is considered acceptable since the concrete core would mainly be loaded in compression.

5. F.E. model validation

The F.E. models have been validated against the test results using the criteria of agreement with failure load, agreement with failure mode and agreement with experimental strain gauge readings. The results are presented separately for ambient and elevated temperature tests.

5.1 Ambient test model validation

The experimental and numerical results for failure load of the ambient tests are depicted in Table 4. The numerical results for failure load compare excellently with the experimental results with a maximum difference of 4.8%.

5.2 Failure mode comparison

In order to compare the failure modes of the tests with those of the numerical results, criteria for failure mode in the F.E. models was required. As the maximum stress of the model is defined by the assigned stress-strain curve the region of maximum strain in each model was compared with the region of failure observed in the experimental tests. For each test it was noted that the region of maximum strain at failure in the corresponding F.E. model strongly correlated to the failure mode of the physical test. As an example of this, Fig. 13 depicts the region of maximum strain in the F.E. model representing test A1. To clarify the difference in strain shown in Fig. 13 for the fin-plate node immediately adjacent to

Table 4 Comparison of experimental and numerical failure loads for ambient tests

Test no.	Test failure load, T_L (kN)	F.E. failure load, A_L (kN)	T_L / A_L
A1	94.6	99.4	0.952
A2	163.7	165	0.992
A3	92.5	94.1	0.983
A4	127.4	128	0.995
A5	69.7	67.3	1.036

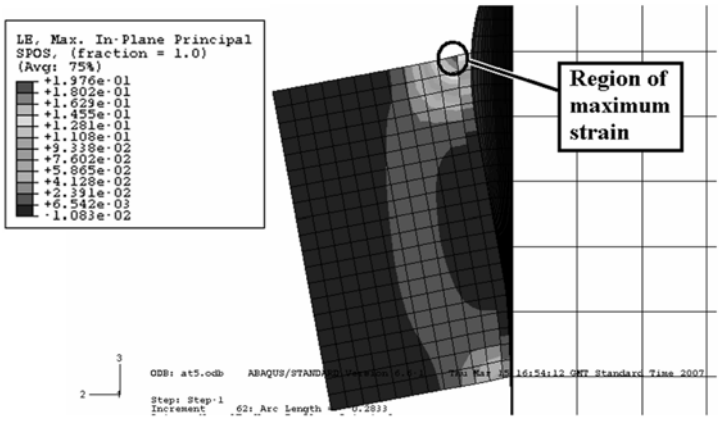

Fig. 13 Region of maximum strain for F.E. model of test A1

the column face and the circled node, Fig. 14 depicts the load vs. strain profiles for these two nodes, denoted (a) and (b) respectively. It may be seen that the maximum strain corresponding to ultimate stress in the stress-strain profile occurs in the circled node of Fig. 13. This nodal position is the point at which the simulated weld section of the fin-plate ends and the fin-plate begins. The maximum strain region in Fig. 13 that is precisely where failure in the experimental test began, as indicated in Table 1.This good correlation of the region of maximum strain in the numerical model with experimental failure mode was observed for all tests.

5.3 Strain comparison

As 13 strain gauges each were used on specimens A1 through A5 a large body of load vs. strain data has been compiled. Some of these results have been reported in Jones & Wang (2007) and, due to the large body of data, they are not fully reproduced in this paper. However, Figs. 15~17 depict load vs. strain profile comparison between test and F.E. results which demonstrate the close correlation of the

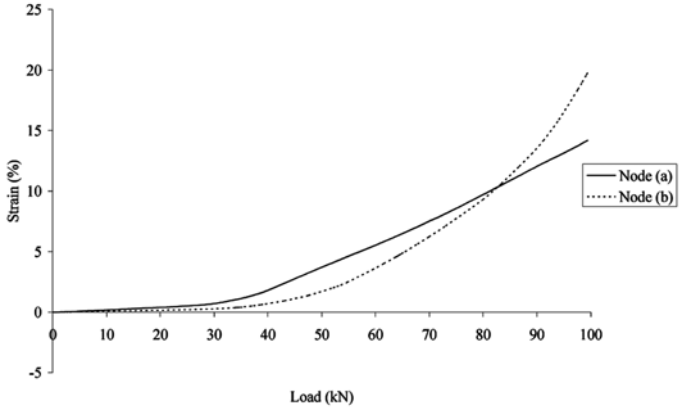

Fig. 14 Strain comparison fin-plate nodes

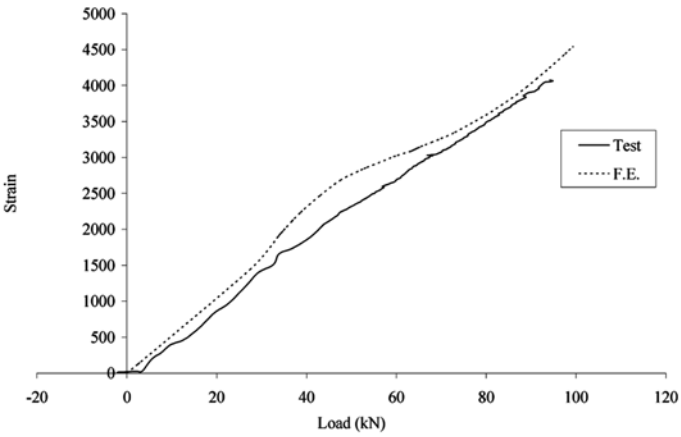

Fig. 15 Load vs. strain comparison for gauge 1, test A1

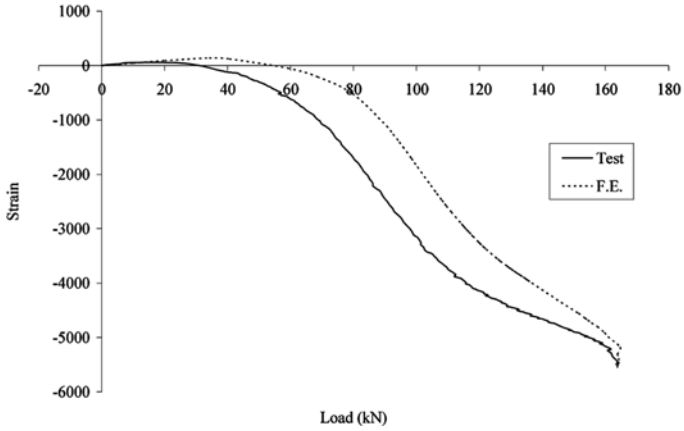

Fig. 16 Load vs. strain comparison for gauge 3, test A2

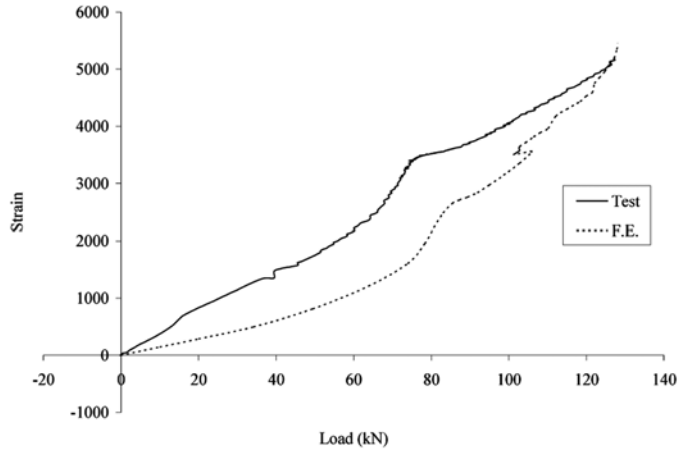

Fig. 17 Load vs. strain comparison for gauge 6, test A4

results. The numerical results show good agreement with the test results across the range of test gauge positions considering that numerical results may only be extracted from discrete nodes which may not fall in the exact position of the experimental gauge due to human error when attaching the gauges. Particularly in regions of high stress the strain was observed to vary significantly over small distances. Despite this, the numerical results agree well with the experiments across the range of gauge positions analyzed.

5.4 Load vs. deflection comparison

The load vs. deflection profiles of the end of the fin-plate connection are compared for both the experimental and numerical cases, as shown in Fig. 18 for the square section and Fig. 19 for the circular section ambient tests. Good correlation between the load vs. deflection was observed for all ambient

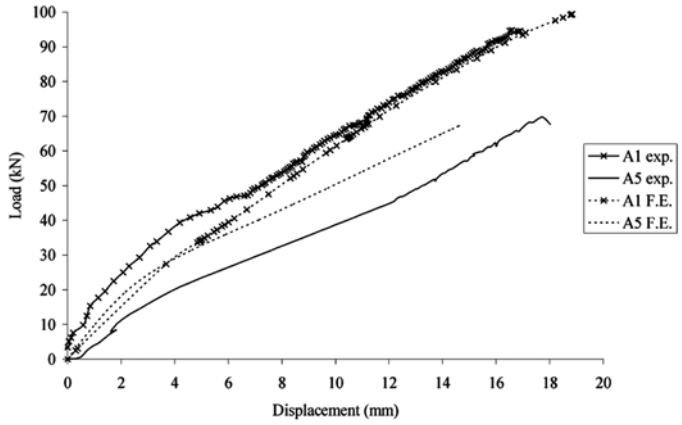

Fig. 18 Load vs. displacement (tests A1 & A5)

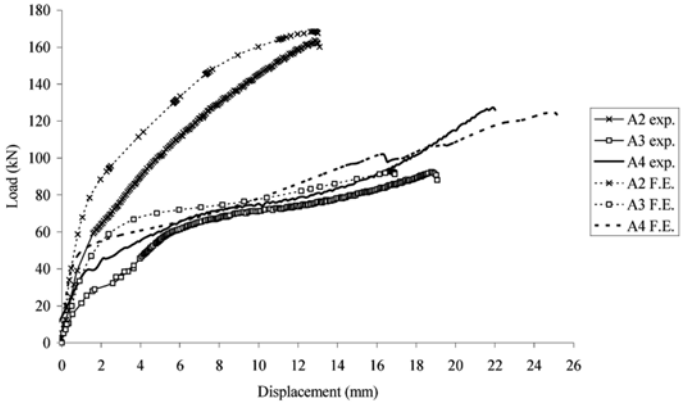

Figure 19. Load vs. displacement (tests A2, A3 & A4)

tests. The maximum displacement of the connection perpendicular to the column face and the point of $3\%b_0$ deformation for tests A1 and A5 is marked on Fig. 20 to illustrate that the load at this point is significantly less than the actual failure load of the connection. Load vs. deflection profiles for elevated temperature tests are discussed in Section 5.5 of this report.

5.5 Elevated temperature test model validation

The elevated temperature tests were performed as steady-state tests. The attached thermocouples were monitored to ensure that the desired test temperature was kept constant throughout the test. When modeling steel for the elevated temperature tests it is necessary to take account of the reduction in strength of the steel at the higher temperatures. Eurocode 3 contains guidance for this through a table of reduction factors applying to the proportional yield strength, the ultimate yield strength and the elastic modulus of the steel for a range of temperatures from ambient to 1,100°C. Table 5 depicts the comparison between experimental and numerical results when the Eurocode reduction factors are applied

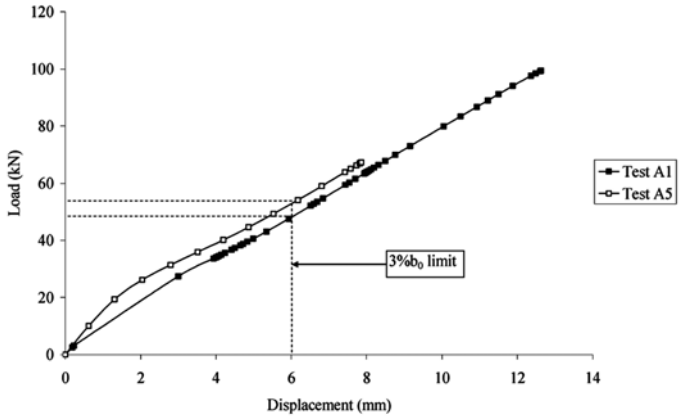

Fig. 20 3%b_0 deformation position (tests A1 & A5)

Table 5 Comparison of experimental and numerical failure loads for elevated temperature tests using Eurocode reduction factors

Test no.	Test Temperature (°C)	Test failure load, T_L (kN)	F.E. failure load, A_L (kN)	T_L/A_L
T1	400	130.7	128	1.021
T2	600	51.1	64	0.798
T3	600	49.6	60.2	0.824
T4	500	85.5	106	0.807
T5	400	133.8	134	0.998
T6	600	53.3	62.1	0.858
T7	600	67.4	67.3	1.001
T8	400	133.4	140	0.953

to the F.E. material model.

It may be observed from Table 5 that the correlation between experimental and F.E. results when applying the Eurocode reduction factors for steel at elevated temperatures is erratic. Whilst good agreement is achieved for tests T1, T5, T7 and T8 the agreement for the other tests is inferior. Tests T2, T3, T4 and T6 all failed at loads some 80~85% of the F.E. failure load.

Alternative investigations to Eurocode into the reduction in strength of steel at elevated temperatures may be found in published literature. Li *et al.* (2003) performed tests upon Chinese grade 16Mn steel (equivalent to European grade S355J2H) at elevated temperatures and reported results which indicate greater reductions in steel strength at elevated temperatures than Eurocode. Table 6 shows the comparison between Eurocode and the findings of Li *et al.* for the reduction factors $k_{y,\theta}$ and $k_{E,\theta}$ where:

$$k_{y,\theta} = f_{y,\theta}/f_y \tag{7}$$

$$k_{E,\theta} = E_{,\theta}/E \tag{8}$$

in which the subscript, θ, denotes the value at elevated temperature.

Table 6 shows that Li *et al.* observed a reduction in the steel ultimate strength, f_y, relative to Eurocode and a relative increase in elastic modulus, E. The results presented in Table 7 indicate that incorporating

Table 6 Comparison of reduction factors for steel at elevated temperatures

Temperature (°C)	Eurocode		Li *et al.* (2003)	
	$k_{y,\theta}$	$k_{E,\theta}$	$k_{y,\theta}$	$k_{E,\theta}$
20	1	1	1	1
400	1	0.7	0.85	0.89
500	0.78	0.6	0.62	0.80
600	0.47	0.31	0.38	0.64

the reduction factors observed by Li *et al.* into the F.E. model gives good agreement with the observed experimental failure load for seven of the eight test specimens. The agreement is more consistent than when using the Eurocode reduction factors. Outinen (2007) also carried out tests upon a range of steel grades to determine their properties at elevated temperatures. Reduction factors inferred from Outinen's tests on S355 steel were incorporated into the F.E. model for the fin-plate section of the model. Similarly, reduction factors from Outinen for S355J2H steel were incorporated into the tube section of the numerical models. The reduction factors from Outinen for both these steel grades are compared with Eurocode in Table 8. As can be seen from Table 8, for steel grade S355J2H Outinen's results were identical to Eurocode for $k_{E,\theta}$ yet for the value of $k_{y,\theta}$ (the reduction in steel strength) was similar to that observed by Li *et al*. For steel grade S355 the values for $k_{y,\theta}$ are similar with a marked reduction in Outinen for values of $k_{E,\theta}$. Table 9 depicts the load comparison between experimental and numerical results when the reduction factors observed by Outinen are incorporated into the F.E. model.

It will be observed from Tables 7 and 9 that incorporating reduction factors other than those recommended by Eurocode into the numerical model significantly affects the results. The agreement between experimental and numerical results with these alternative reduction factors is generally good although the correlation in table 7 for test T7 is quite poor. Although the results in table 9 were predicated upon assuming a steel grade of S355 for the fin-plate section, the actual steel grade of the fin-plate sections of the test specimens could not be traced. The steel grade of the columns was known to be S355J2H and therefore using either Li or Outinen reduction factors for this part of the numerical model was justified. The load vs. deflection curves for the elevated temperature numerical models compare well with those from experiments when using reduction factors from Outinen (2007). Fig. 21 depicts typical comparisons for elevated temperature tests T3 and T5.

Table 7 Comparison of experimental and numerical failure loads for elevated temperature tests using Li *et al.* (2003) reduction factors

Test no.	Test Temperature (°C)	Test failure load, T_L (kN)	F.E. failure load, A_L (kN)	T_L / A_L
T1	400	130.7	119	1.099
T2	600	51.1	56.1	0.911
T3	600	49.6	50.7	0.979
T4	500	85.5	89.4	0.956
T5	400	133.8	129	1.038
T6	600	53.3	49.5	1.077
T7	600	67.4	56.6	1.190
T8	400	133.4	127	1.050

Table 8 Further comparison of reduction factors for steel at elevated temperatures

Temperature (°C)	Eurocode		S355 (Outinen 2007)		S355J2H (Outinen 2007)	
	$k_{y,\theta}$	$k_{E,\theta}$	$k_{y,\theta}$	$k_{E,\theta}$	$k_{y,\theta}$	$k_{E,\theta}$
20	1	1	1	1	1	1
400	1	0.7	0.89	0.61	0.85	0.7
500	0.78	0.6	0.73	0.47	0.65	0.6
600	0.47	0.31	0.47	0.29	0.32	0.31

Table 9 Comparison of experimental and numerical failure loads for elevated temperature tests using Outinen (2007) reduction factors

Test no.	Test Temperature (°C)	Test failure load, T_L (kN)	F.E. failure load, A_L (kN)	T_L / A_L
T1	400	130.7	143	0.914
T2	600	51.1	55.7	0.917
T3	600	49.6	56.8	0.873
T4	500	85.5	92.5	0.924
T5	400	133.8	129.5	1.033
T6	600	53.3	50.7	1.051
T7	600	67.4	58.9	1.144
T8	400	133.4	139	0.960

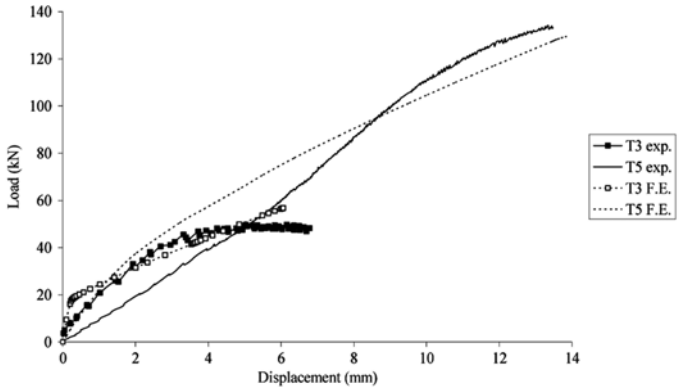

Fig. 21 Load vs. displacement (tests T3 & T5)

6. Future method for evaluating column strength

This paper has presented experimental results of fin-plate to CFT column connections under shear and bending load. A need has been identified for a solution method which calculates the strength of the column component under such load. The strength of fin-plates under shear and bending load, without the influence of the steel tube, is already well documented. Further research should be focused on behavior of the tube.

Before attempting to develop a solution method for the tubular column strength under shear and bending load, the simpler case of purely tensile load should first be evaluated. This is because failure of the steel tube under a shear load in the fin plate is caused by tension of the steel tube in the circumferential direction of the steel tube. As has been discussed in the introduction to this paper,

previous approaches to this problem have taken the form of applying a deformation limit to the column face and subsequently curve-fitting numerical results with respect to a yield line mechanism. However, this approach may be inadequate as it does not calculate the ultimate failure load nor does the yield line mechanism necessarily develop fully. Potential membrane action is also not considered.

7. Summary

This paper has presented the results of an experimental study of the shear behavior of fin-plates welded to steel tubes at ambient and elevated temperatures. A numerical model based on the finite element method is also presented and has been validated against the test data. Based on the results of this study the following main conclusions may be drawn:

- Two failure modes were observed: fracture of the fin plate at the weld position and tearing out of the tube around the weld in the tension zone.
- Concrete in-fill has been observed to influence the failure mode for otherwise similar connections. Concrete in-fill significantly increases the strength of welded fin-plate to CFT connections. This is attributed to a change in moment arm along the connection length.
- Connections to circular tubes have higher resistance than connections to square tubes. Even when the failure mode of the connection is in the fin plate, it is not adequate to use the Eurocode 3 method to calculate the connection strength, based on shear and bending moment interaction. The steel tube affects the fin plate behavior and this should be considered in design.
- The current design method in CIDECT guide 9, based on a deflection limit of 3% of the tube width, can severely underestimate the connection strength, because it fails to take into consideration membrane action in the steel tube.
- The numerical model developed for each ambient specimen configuration has been shown to agree well with the experimental failure load and strain profiles.
- The numerical results agree well with experimental results at elevated temperatures when applying reduction factors similar to those observed by Li *et al*. (2003) or Outinen (2007) for the steel tubes and the Eurocode 3 reduction factors for the T-stub (fin plate).
- It is possible to determine the failure mode of numerical models by observing the region of maximum strain at failure.

Acknowledgments

This work was made possible by the sponsorship of an EPSRC industrial CASE award to the first author in which the industrial partner is Corus Tubes. The authors would like to thank Mr. Andrew Orton of Corus Tubes for his interest in the research. Thanks are also due to Mr. Jim Gee and the other technicians of the Structures Division, University of Manchester, for fabricating the test specimens and assisting with the tests.

References

Cao, J. J., Packer, J. A. & Yang, G. J. (1998), "Yield line analysis of RHS connections with axial loads". *J.*

Constr. Steel Res., **Vol. 48**, pp.1-25.
CEN. 2001. Eurocode 3: Design of steel structures, Part 1.2: General rules – structural fire design. Draft for development, European committee for standardization. Document DD ENV 1993-1-2: 2001.
CEN. 2003. Eurocode 3: Design of steel structures, Part 1.8: Design of joints. European committee for standardization. Document prEN 1993-1-8: 2003.
FEMA (Federal Emergency Management Agency) (2002). *World Trade Center Building Performance Study: Data Collection, Preliminary Observations and Recommendations*. Greenhorne & O'Mara, Inc.
Hibbitt, Karlsson & Sorensen, inc. 2004. ABAQUS manuals version 6.4. Providence RI, USA.
Jones, M. H. & Wang, Y. C. (2006), "Shear behavior of fin plates to tubular columns at ambient and elevated temperatures". *Proc. 11th International Symposium on Tubular Structures, Tubular Structures X1, Packer & Willibald (eds.), Quebec City, Canada.* pp 425-432.
Jones, M. H. & Wang Y. C. (2007), "Experimental studies and numerical analysis of the shear behavior of fin plates to tubular columns at ambient and elevated temperatures", *Proc. 3rd International Conference on Steel and Composite Structures, Wang & Choi (eds.), Manchester, U.K.* pp 557-564.
Kostecki, N. & Packer, J. A. (2003), "LongItudinal plate and through plate-to-hollow structural section welded connections", *J. Struct. Eng.*, American Society of Civil Engineers, 10.1061/(ASCE)0733-9445, 129:4 (478).
Kurobane, Y., Packer, J. A., Wardenier, J. & Yeomans, N. (2004), Design guide for structural hollow section column connections, CIDECT Design Guide 9 for Construction with Hollow Steel Sections. TÜV-Verlag.
Li, G. Q., Jiang, S. C., Yin, Y. Z., Chen, K. & Li, M. F. (2003), "Experimental Studies on The Properties of Constructional Steel at Elevated Temperatures", *J. Struct. Eng*, American Society of Civil Engineers, 10.1061/(ASCE)0733-9445, 129:12 (1717).
Lu, L. H. (1997), "The static strength of I-beam to rectangular hollow section column connections", PhD thesis, University of Delft, Delft University Press, Netherlands.
Outinen, J. (2007), "Mechanical properties of structural steels at high temperatures and after cooling down", PhD Thesis, Helsinki University of Technology, Laboratory of Steel Structures Publications 32, Helsinki, Finland.
Packer, J. J. & Henderson. J. E. (1997), *Hollow structural section connections and trusses: a design guide, 2nd Ed.*, Canadian Institute of Steel Construction.
Sherman, D. R. (1995), "Simple Framing Connections to HSS Columns", *Proc. American Institute of Steel Construction, National steel construction conference, San Antonio, Texas, USA*. 30.1-30.16.
Wang, Y.C. 2002. *Steel and Composite Structures, Behaviour and Design for Fire Safety*, Spon Press.
White, R. N. & Fang, P. J. (1966), "Framing Connections for Square Structural Tubing". *J. Struct. Div*, American Society of Civil Engineers 92(ST2): 175-194.
Yamamoto, N., Inaoka, S. & Morita, K. (1994), "Strength of un-stiffened connection between beams and concrete filled tubular column", *Proc. 6th International Symposium on Tubular Structures, Tubular Structures V1, Grundy, Holgate & Wong (eds.), Rotterdam, Netherlands.* pp 365-372.

YW